PNAS

Supplementary Information for
Observation of high-order imaginary Poynting momentum optomechanics in structured light

Yuan Zhou[†], Xiaohao Xu[*†], Yanan Zhang, Manman Li, Shaohui Yan[*], Manuel Nieto-Vesperinas, Baojun Li, Cheng-Wei Qiu[*], and Baoli Yao[*]

*Xiaohao Xu, Shaohui Yan, Cheng-Wei Qiu, and Baoli Yao
Email: xuxhao_dakuren@163.com, shaohuiyan@opt.ac.cn, chengwei.qiu@nus.edu.sg, yaobl@opt.ac.cn
†These authors contributed equally to this work.

This PDF file includes:

Other supplementary materials for this manuscript include the following:

Supplementary Information Text

Note 1. Derivation of the expression for the complex Poynting vector of the focused cylindrical vector (CV) field.

The focusing geometry is illustrated in Fig. 1a in the main text. An input CV field,

$$\mathbf{A}_0(\varrho,\varphi) = \left(\cos\alpha\mathbf{e}_\varrho + \sin\alpha\mathbf{e}_\varphi\right)\mathcal{A}_0(\vartheta), \tag{S1.1}$$

is focused by a high numerical aperture (NA) objective lens. Upon apodization, the field takes on a spherical wave front of radius f (the focal length of the objective lens) with amplitude

$$\mathbf{A}_1(\vartheta,\varphi) = \sqrt{\cos\vartheta}\left(\cos\alpha\mathbf{e}_p + \sin\alpha\mathbf{e}_s\right)\mathcal{A}_0(\vartheta) \tag{S1.2}$$

where $\mathbf{e}_s = \mathbf{e}_\varphi$ and $\mathbf{e}_p$ is obtained by deflecting $\mathbf{e}_\varrho$ by ϑ, the angle between the deflected light ray and the z-axis. In terms of Cartesian coordinate basis ($\mathbf{e}_x$, $\mathbf{e}_y$, $\mathbf{e}_z$), the unit vectors $\mathbf{e}_p$ and $\mathbf{e}_s$ are

$$\begin{aligned}\mathbf{e}_p &= \cos\vartheta\cos\varphi\mathbf{e}_x + \cos\vartheta\sin\varphi\mathbf{e}_y + \sin\vartheta\mathbf{e}_z,\\ \mathbf{e}_s &= -\sin\varphi\mathbf{e}_x + \cos\varphi\mathbf{e}_y,\end{aligned} \tag{S1.3}$$

and the unit propagation vector

$$\hat{\mathbf{k}} = k\mathbf{e}_p \times \mathbf{e}_s = -\sin\vartheta\cos\varphi\mathbf{e}_x - \sin\vartheta\sin\varphi\mathbf{e}_y + \cos\vartheta\mathbf{e}_z. \tag{S1.4}$$

By the Richards-Wolf integral, the focused electric and magnetic fields in the vicinity of the focus then reads (S1, S2)

$$\begin{Bmatrix}\mathbf{E}(\mathbf{x})\\ \mu c\mathbf{H}(\mathbf{x})\end{Bmatrix} = -\frac{ikf}{2\pi}\int_0^{\Theta}\sin\vartheta d\vartheta\int_0^{2\pi}\begin{Bmatrix}\mathbf{A}_1(\vartheta,\varphi)\\ \hat{\mathbf{k}}\times\mathbf{A}_1(\vartheta,\varphi)\end{Bmatrix}e^{i\mathbf{k}\cdot\mathbf{x}}d\varphi, \tag{S1.5}$$

where $\mathbf{k} = k\hat{\mathbf{k}}$ and $\mathbf{x}$ is the position vector of observation point that has components (ρ, ϕ, z) in the cylindrical coordinate system holding the focus.

On substitution of [S1.2] – [S1.4] into [S1.5] and making change of integration variables $\varphi \longrightarrow \varphi + \pi$, we have for the focused electric field

$$\mathbf{E}(\mathbf{x}) = \frac{ikf}{2\pi}\int_0^{\Theta}\sqrt{\cos\vartheta}\mathcal{A}_0(\vartheta)\sin\vartheta d\vartheta\int_0^{2\pi}\begin{Bmatrix}(\cos\alpha\cos\vartheta\cos\varphi - \sin\alpha\sin\varphi)\mathbf{e}_x\\ +(\cos\alpha\cos\vartheta\sin\varphi + \sin\alpha\cos\varphi)\mathbf{e}_y\\ -\cos\alpha\sin\vartheta\mathbf{e}_z\end{Bmatrix}e^{i\mathbf{k}\cdot\mathbf{x}}d\varphi, \tag{S1.6}$$

where the propagation vector $\mathbf{k}$ is

$$\mathbf{k} = k\left(\sin\vartheta\cos\varphi\mathbf{e}_x + \sin\vartheta\sin\varphi\mathbf{e}_y + \cos\vartheta\mathbf{e}_z\right). \tag{S1.7}$$

The basis vectors ($\mathbf{e}_\rho$, $\mathbf{e}_\phi$, $\mathbf{e}_z$) for cylindrical coordinates are related to Cartesian coordinate basis vectors by the transformations

$$\begin{aligned}\mathbf{e}_\rho &= \cos\phi\mathbf{e}_x + \sin\phi\mathbf{e}_y,\\ \mathbf{e}_\phi &= -\sin\phi\mathbf{e}_x + \cos\phi\mathbf{e}_y,\end{aligned} \tag{S1.8}$$

with $\mathbf{e}_z$ vector unchanged. Thus, the dot product of $\mathbf{k}$ and the position vector $\mathbf{x}$ is

$$\mathbf{k}\cdot\mathbf{x} = k\rho\sin\vartheta\cos(\phi-\varphi) + kz\cos\vartheta.$$

Note that the basis vectors, $\mathbf{e}_\rho$ and $\mathbf{e}_\phi$, are independent of the integration variables ϑ and φ. In changing to the cylindrical coordinate basis, Eq. [S1.6] becomes

$$\begin{aligned}\mathbf{E}(\mathbf{x}) = \frac{ikf}{2\pi}&\int_0^{\Theta}\sqrt{\cos\vartheta}\mathcal{A}_0(\vartheta)\sin\vartheta d\vartheta\\ &\times\int_0^{2\pi}\begin{Bmatrix}[\cos\alpha\cos\vartheta\cos(\phi-\varphi) + \sin\alpha\sin(\phi-\varphi)]\mathbf{e}_\rho\\ -[\cos\alpha\cos\vartheta\sin(\phi-\varphi) - \sin\alpha\cos(\phi-\varphi)]\mathbf{e}_\phi\\ -\cos\alpha\sin\vartheta\mathbf{e}_z\end{Bmatrix}e^{i\mathbf{k}\cdot\mathbf{x}}d\varphi.\end{aligned} \tag{S1.9}$$

Applying the integral representation for cylindrical Bessel functions

$$\begin{aligned}&\int_0^{2\pi}e^{i\eta\cos(\phi-\varphi)}d\varphi = 2\pi J_0(\eta),\\ &\int_0^{2\pi}\cos(\phi-\varphi)e^{i\eta\cos(\phi-\varphi)}d\varphi = i2\pi J_1(\eta),\\ &\int_0^{2\pi}\sin(\phi-\varphi)e^{i\eta\cos(\phi-\varphi)}d\varphi = 0,\end{aligned}$$

the integration over φ in [S1.9] can be analytically carried out, yielding

$$\mathbf{E}(\mathbf{x}) = -kf\int_0^{\Theta}\sqrt{\cos\vartheta}\,\mathcal{A}_0(\vartheta)\begin{Bmatrix}\cos\alpha\cos\vartheta J_1(k\rho\sin\vartheta)\mathbf{e}_\rho\\ +\sin\alpha J_1(k\rho\sin\vartheta)\mathbf{e}_\phi\\ +i\cos\alpha\sin\vartheta J_0(k\rho\sin\vartheta)\mathbf{e}_z\end{Bmatrix}e^{ikz\cos\vartheta}\sin\vartheta d\vartheta\,. \qquad [S1.10]$$

Letting

$$U(\rho,z) = -kf\int_0^{\Theta}\sqrt{\cos\vartheta}\,\mathcal{A}_0(\vartheta)J_1(k\rho\sin\vartheta)e^{ikz\cos\vartheta}\sin\vartheta d\vartheta\,, \qquad [S1.11]$$

the electric field **E** can be written in a concise form as Eq. [2] in the main text:

$$\mathbf{E}(\mathbf{x}) = -i\frac{\cos\alpha}{k}\partial_z U(\rho,z)\mathbf{e}_\rho + U(\rho,z)\sin\alpha\mathbf{e}_\phi + i\frac{\cos\alpha}{k}\left(\partial_\rho + \frac{1}{\rho}\right)U(\rho,z)\mathbf{e}_z\,. \qquad [S1.12]$$

In passing from [S1.10] to [S1.11], we have made use of the following recurrence relation

$$\left(\partial_\rho + \frac{1}{\rho}\right)J_1(k\rho\sin\vartheta) = k\sin\vartheta J_0(k\rho\sin\vartheta)\,. \qquad [S1.13]$$

From Eq. [S1.5], we see that the scaled magnetic field $\mu c\mathbf{H}$ can be obtained from the **E**-field merely by a replacement: $\alpha \longrightarrow \alpha + \pi/2$; we thus have

$$\mu c\mathbf{H}(\mathbf{x}) = i\frac{\sin\alpha}{k}\partial_z U(\rho,z)\mathbf{e}_\rho + \cos\alpha U(\rho,z)\mathbf{e}_\phi - i\frac{\sin\alpha}{k}\left(\partial_\rho + \frac{1}{\rho}\right)U(\rho,z)\mathbf{e}_z\,. \qquad [S1.14]$$

With Eqs. [S1.12] and [S1.14], direct calculation of the complex Poynting momentum $\mathbf{\Pi} = (\mathbf{E}^* \times \mathbf{H})/2$ results in

$$\begin{aligned}\mathbf{\Pi} = \frac{1}{2\mu c}\Bigg\{ & i\left[\frac{\cos^2\alpha}{k}U\frac{\partial}{\rho\partial\rho}\left(\rho U^*\right) - \frac{\sin^2\alpha}{k}U^*\frac{\partial}{\rho\partial\rho}(\rho U)\right]\mathbf{e}_\rho \\ & + i\frac{\sin 2\alpha}{k^2}\mathrm{Im}\left[\frac{\partial U}{\partial z}\frac{\partial}{\rho\partial\rho}\left(\rho U^*\right)\right]\mathbf{e}_\phi + i\frac{\cos^2\alpha U\left(\partial_z U^*\right) - \sin^2\alpha U^*\left(\partial_z U\right)}{k}\mathbf{e}_z\Bigg\}.\end{aligned} \qquad [S1.15]$$

whose imaginary part evaluated at the focal plane ($z = 0$) gives Eq. [4] in the main text.

Note 2. Analysis on photophoretic effects calculations.

The photophoretic force arises from the light-induced uneven temperature increase on the particle's surface. Figures S1a and b show the simulated field distribution around the particle for IRT and ORT, respectively. The nonuniform field leads to inhomogeneous temperature increase $\Delta T = T - T_0$, which is shown in Figs. S1c and d. Here, T_0 = 298 K is the room temperature and T is calculated by solving the steady-state heat transfer equation (S3):

$$-\kappa\nabla^2 T = \frac{1}{2}\omega\,\mathrm{Im}\left(\varepsilon_g\right)|\mathbf{E}|^2\,, \qquad [S2.1]$$

where ω is the angular frequency of the field, ε_g the permittivity of gold, and C is the space-dependent thermal conductivity of material ($\kappa = \kappa_g$ = 317 $\mathrm{Wm^{-1}K^{-1}}$ for the gold particle and $\kappa = \kappa_w$ = 0.6 $\mathrm{Wm^{-1}K^{-1}}$ for water). In the calculations, we have assumed $T = T_0$ (room temperature) at infinity and used continuous conditions at the particle-water interface:

$$\kappa_g\mathbf{n}\cdot\nabla T_g = \kappa_w\mathbf{n}\cdot\nabla T_w \text{ and } T_g = T_w\,. \qquad [S2.2]$$

where T_g and T_w represent the temperature of particle and water. Eventually, the photophoretic force in the azimuthal direction is evaluated using the formula (S4): $F_\mathrm{ph} = -15/(64\sqrt{2})k_B/\sigma_{cs}\cdot\alpha\cdot dT/dy\cdot S_v$, where k_B is the Boltzmann's constant, $\sigma_{cs} = \pi\times(0.4\text{ nm})^2 = 5.0\times10^{-19}$ m^2, and $a = 0.8$ is the thermal accommodation at T_0. We assume the active thermal creep flow region to be the particle's diameter: L = 1.5 μm. For the IRT and ORT, the photophoretic forces are calculated respectively to be F_ph = 1.4 and −0.5 pN/W, which are much smaller than the optical force F. Moreover, F_ph acts in the opposite direction to F.

Note 3. Shaping the IPM vortex by modulating the input CV field

From the expression [S1.15] for the complex Poynting vector $\mathbf{\Pi}$, we see that its azimuthal component Π_ϕ is purely imaginary throughout the focal region, regardless of the concrete form of the input amplitude $\mathcal{A}_0(\vartheta)$

at the entrance pupil. Furthermore, because Π_ϕ is ϕ-independent, the focused field can have the azimuthal IPM at every azimuthal position, that is, an imaginary Poynting momentum vortex (IPMV). A simple scheme to detect such IPMV is to place a particle probe in the focused field and to observe the particle's orbital rotation.

To excite the high-order IPM force, the particles in our experiment are chosen as gold spheres of average radius of ~0.75 μm (1.5 μm in diameter). With such particle size, the particles can be easily imaged using conventional imaging system. However, the detection of particle's orbital motion with a standard CV input amplitude (S5) is not easy, because such input field will lead to a focusing spot of very small size, as shown in Fig. S2a. We see that the intensity pattern in the focal plane for each polarization parameter (α = 0, –22.5 or –45°) is of spot-like shape with size ~λ. Also, the IPM flow (Fig. S2b) is shown to be concentrated to this region. Given that the gold spheres used in our experiment have an average diameter of 1.5 μm, the center of the particle being trapped will almost coincide with the beam axis, so that it is difficult to distinguish the particle's orbital motion in experiments.

A solution to this problem is to create an annular focusing pattern with the ring radius much larger than that of the particle. The generation of the annular pattern with tunable radius can be achieved by the so-called perfect vortex technique, the underlying idea of which is to introduce a non-constant phase modulation function. In our work, we take the phase modulation function shown in Eq. [8] to yield a higher power utilization, and put the modulation factor ρ_0 = 5.5 μm. Consequently, we can obtain an annular intensity pattern in the focal plane of radius ~ρ_0, as shown in Fig. S2c. Such focusing property can be understood by noting that the focused field in the focal plane is the inverse Fourier transform of the input field (see Eq. [S1.5]); the Fourier transform of $J_0(k\rho_0 \sin\vartheta)$ is just a ring of radius ~ρ_0. Additionally, we see that the azimuthal IPM now is far away from the beam axis (Fig. S2d). The field thus permit the clear observation of the particle's rotational behavior due to the IPM vortex (see Figs. 3b and 4).

Note 4. Expressing optical forces in terms of flows via the multipole expansion technique

The time-averaged optical force on a homogenous, isotropic spherical particle can be calculated in a rigorous way by combining the Mie theory with the Maxwell stress tensor method. In the Mie theory, the incident and scattered fields are expanded in terms of vector spherical wave functions (VSWFs) (S6):

$$\begin{aligned}\mathbf{E}(\mathbf{x}) &= E_0 \sum_{l=1}^{N_{\max}} \sum_{m=-l}^{l} \left[a_{l,m}\, \mathrm{Rg}\,\mathbf{M}_{l,m}(k\mathbf{x}) + b_{l,m}\, \mathrm{Rg}\,\mathbf{N}_{l,m}(k\mathbf{x}) \right], \\ \boldsymbol{\mathcal{E}}(\mathbf{x}) &= E_0 \sum_{l=1}^{N_{\max}} \sum_{m=-l}^{l} \left[p_{l,m}\mathbf{M}_{l,m}(k\mathbf{x}) + q_{l,m}\mathbf{N}_{l,m}(k\mathbf{x}) \right],\end{aligned} \qquad [S4.1]$$

where Rg$\mathbf{M}_{l,m}$ and Rg$\mathbf{N}_{l,m}$ are the first kind of VSWFs with respect to which the incident field are expanded with coefficients $a_{l,m}$ and $b_{l,m}$; $\mathbf{M}_{l,m}$ and $\mathbf{N}_{l,m}$ are the third kind of VSWFs with $p_{l,m}$ and $q_{l,m}$ denoting the corresponding expansion coefficients for scattered field. The scattering coefficients are related to the incident coefficients through the Mie coefficients (A_l, B_l):

$$p_{l,m} = -B_l a_{l,m}, \quad q_{l,m} = -A_l b_{l,m}.$$

The first kind of VSWFs Rg$\mathbf{M}_{l,m}$ and Rg$\mathbf{N}_{l,m}$, in spherical coordinates (r, θ, ϕ), are given by

$$\left.\begin{matrix}\mathrm{Rg}\,\mathbf{M}_{l,m}(k\mathbf{x}) \\ \mathrm{Rg}\,\mathbf{N}_{l,m}(k\mathbf{x})\end{matrix}\right\} = D_{lm} \begin{cases} j_l(kr)\mathbf{C}_{l,m}(\theta,\phi) \\ \dfrac{l(l+1)}{kr}\, j_l(kr)\mathbf{P}_{l,m}(\theta,\phi) + \dfrac{\left[krj_l(kr)\right]'}{kr}\mathbf{B}_{l,m}(\theta,\phi) \end{cases}, \qquad [S4.2]$$

where $j_l(\cdot)$ is the first kind of spherical Bessel function of order l and

$$D_{lm} = \sqrt{\frac{(2l+1)}{4\pi l(l+1)}\frac{(l-m)!}{(l+m)!}},$$

In the above formulae vector spherical harmonic functions are defined as (S6)

$$\begin{aligned}\mathbf{P}_{l,m}(\theta,\phi) &= \mathbf{e}_r P_l^m(\cos\theta) e^{im\phi}, \\ \mathbf{B}_{l,m}(\theta,\phi) &= \left[\mathbf{e}_\theta \frac{d}{d\theta} P_l^m(\cos\theta) + \mathbf{e}_\phi \frac{im}{\sin\theta} P_l^m(\cos\theta) \right] e^{im\phi}, \\ \mathbf{C}_{l,m}(\theta,\phi) &= \left[\mathbf{e}_\theta \frac{im}{\sin\theta} P_l^m(\cos\theta) - \mathbf{e}_\phi \frac{d}{d\theta} P_l^m(\cos\theta) \right] e^{im\phi},\end{aligned} \qquad [S4.3]$$

with $P_l^m(\cdot)$ referring to associated Legendre functions. The third kind of VSWFs $\mathbf{M}_{l,m}(k\mathbf{x})$ and $\mathbf{N}_{l,m}(k\mathbf{x})$ are defined in the same way as [S4.2] with $h_l(kr)$ in place of $j_l(kr)$.

Usually the incident coefficients are known, from which the scattering coefficients are calculated and so are the scattered fields. Having obtained the scattered fields by the Mie theory, the time-averaged optical force $\mathbf{F}$ on the particle can be computed by integrating the Maxwell stress tensor (MST) $\mathbf{T}^{(2)}$ (Minkowski form) over a closed surface enclosing the particle (S7):

$$\mathbf{F} = \int_{S_\infty} \left\langle \mathbf{T}^{(2)} \right\rangle \cdot \mathbf{n} dS \,. \tag{S4.4}$$

Upon substitution of the VSWFs expansion [S4.1] in [S4.4] and integrating over a spherical surface at infinity, we may obtain, from the orthogonality of spherical harmonics, the force as a series over the incident and scattering coefficients (S8). This series allows us to evaluate the force components arising from multipoles of arbitrary order, but it fails to establish an explicit connection between the force and the illuminating field vectors. To establish such a relation, Cartesian *multipole moment* tensors, instead of the VSWFs, are introduced to represent the fields (S9, S10).

The Cartesian electric and magnetic multipole moments $\mathbb{O}_{\text{elec}}^{(l)}$ and $\mathbb{O}_{\text{mag}}^{(l)}$ of order l are defined by (S9)

$$\mathbb{O}_{\text{elec(mag)}}^{(l)} \equiv \gamma_{\text{elec (mag)}}^{(l)} \sum_{m=0}^{\left\lfloor \frac{l-1}{2} \right\rfloor} d_{l,m} k^{2m} \hat{\mathcal{S}} \left(\overbrace{\mathbb{I} \otimes \mathbb{I} \otimes \cdots \otimes \mathbb{I}}^{m} \otimes \mathbb{M}_{\text{elec (mag)}}^{(l-2m)} \right), \tag{S4.5}$$

where $\lfloor x \rfloor$ gives the greatest integer not larger than x and

$$\gamma_{\text{elec}}^{(l)} = \frac{4l(2l+1)!!}{(l+1)} \frac{i\pi\varepsilon A_l}{k^{2l+1}}, \quad \gamma_{\text{mag}}^{(l)} = \frac{4l(2l+1)!!}{(l+1)} \frac{i\pi B_l}{\mu k^{2l+1}}, \tag{S4.6}$$

represent the electric and magnetic 2^l-polar polarizabilities, respectively; The notation $\hat{\mathcal{S}}$ denotes the symmetrization operator and

$$\begin{aligned} d_{l,m} &= \frac{l!}{4^m m!} \frac{\Gamma(l-m+1/2)}{\Gamma(l+1/2)\Gamma(l-2m)} \frac{1}{l}, \quad d_{l,0} = 1 \\ \mathbb{M}_{\text{elec}}^{(k)} &= \hat{\mathcal{S}}\left(\nabla^{(k-1)}\mathbf{E}\right), \quad \mathbb{M}_{\text{(mag)}}^{(k)} = \hat{\mathcal{S}}\left(\nabla^{(k-1)}\mathbf{B}\right) \end{aligned} \tag{S4.7}$$

with $\Gamma(\cdot)$ being the Gamma function. Equation [S4.7] can be inverted to yield an expression for the fields as a sum over l of $\mathbb{O}_{\text{elec}}^{(l)}$ ($\mathbb{O}_{\text{mag}}^{(l)}$) contracted with some properly chosen tensors. Substituting the resulting expressions into the integrand in [S4.4], one may obtain, after lengthy algebra, an expression for $\mathbf{F}$ in terms of incident field moments given by Eq. [9] in the main text, or Eq. [16] in Ref. (S10).

We have shown in our Eq. [16] that $\mathbf{S}_{\text{em}}^{(n)}$ represents the moment of complex Poynting vector, so the force terms associated with its imaginary part constitutes the IPM force. Based on Eqs. [18] and [21] in Ref. (S10), it is readily to obtain the IPM force derived from all the possible interactions of multipoles with order $l \le N$:

$$\mathbf{F}_{\text{IPM}}^{(N)} = \mathbf{F}_{\text{IPM}}^{\text{e}(N)} + \mathbf{F}_{\text{IPM}}^{\text{m}(N)} + \mathbf{F}_{\text{IPM}}^{\text{x}(N)}, \tag{S4.8}$$

$$\mathbf{F}_{\text{IPM}}^{\text{e}(N)} = \frac{\mu c}{4\pi\varepsilon} \sum_{n=1}^{N} \left\{ \sum_{m=0}^{\left\lfloor \frac{n-2}{2} \right\rfloor} \Lambda_{n-1,m} \operatorname{Im}\left[\gamma_{\text{elec}}^{(n-1)} \gamma_{\text{elec}}^{(n)*} \right] \operatorname{Im} \mathbf{S}_{\text{em}}^{(n-2m-1)} + \sum_{m=0}^{\left\lfloor \frac{n-3}{2} \right\rfloor} \Omega_{n-1,m} \operatorname{Im}\left[\gamma_{\text{elec}}^{(n-1)} \gamma_{\text{elec}}^{(n)*} \right] \operatorname{Im} \mathbf{S}_{\text{em}}^{(n-2m-2)} \right\}, \tag{S4.9}$$

$$\mathbf{F}_{\text{IPM}}^{\text{m}(N)} = -\frac{\mu}{4\pi\varepsilon c^3} \sum_{n=1}^{N} \left\{ \sum_{m=0}^{\left\lfloor \frac{n-2}{2} \right\rfloor} \Lambda_{n-1,m} \operatorname{Im}\left[\gamma_{\text{mag}}^{(n-1)} \gamma_{\text{mag}}^{(n)^*} \right] \operatorname{Im} \mathbf{S}_{\text{em}}^{(n-2m-1)} + \sum_{m=0}^{\left\lfloor \frac{n-3}{2} \right\rfloor} \Omega_{n-1,m} \operatorname{Im}\left[\gamma_{\text{mag}}^{(n-1)} \gamma_{\text{mag}}^{(n)^*} \right] \operatorname{Im} \mathbf{S}_{\text{em}}^{(n-2m-2)} \right\}, \tag{S4.10}$$

$$\mathbf{F}_{\mathrm{IPM}}^{\mathrm{x}(N)}=\frac{\mu}{4\pi\varepsilon c}\sum_{n=1}^{N}\left\{\sum_{m=0}^{\left\lfloor\frac{n-1}{2}\right\rfloor}M_{n,m}\,\mathrm{Im}[\gamma_{\mathrm{elec}}^{(n)*}\gamma_{\mathrm{mag}}^{(n)}]\left[\mathrm{Im}\,\mathbf{S}_{\mathrm{em}}^{(n-2m)}-\frac{(n-2m-1)}{(n-2m)^2}k^2\,\mathrm{Im}\,\mathbf{S}_{\mathrm{em}}^{(n-2m-1)}\right.\right.$$
$$\left.\left.-\frac{(n-2m-1)(n-2m-2)}{(n-2m)^2}k^4\,\mathrm{Im}\,\mathbf{S}_{\mathrm{em}}^{(n-2m-2)}\right]\right\}, \qquad [S4.11]$$

where

$$\begin{aligned}
\Lambda_{n,m}&=\frac{n(n+2)(2n-2m+1)2^{n+1}}{(n-2m)(n+1)(2n+1)(2n+3)!}k^{2n+4m+4}c_{n,m},\\
\Omega_{n,m}&=\Lambda_{n,m}\frac{(n-2m-1)}{(2n-2m+1)}k^2,\\
M_{n,m}&=\frac{2^n}{(2n+1)!}\frac{(n-2m)}{n^2}k^{2n+4m+2}c_{n,m},\\
c_{n,m}&=(-1)^m\frac{(n-2m)}{4^m n^2}\frac{n!}{m!}\frac{\Gamma\left(n-m+\frac{1}{2}\right)}{\Gamma\left(n+\frac{1}{2}\right)\Gamma(n-2m)}.
\end{aligned} \qquad [S4.12]$$

To know the force contribution from the field moment of each order, we may recast Eqs. [S4.9]-[S4.11], with the index substitution method, into

$$\mathbf{F}_{\mathrm{IPM}}^{\mathrm{e}(N)}=\frac{\mu c}{4\pi\varepsilon}\sum_{l=1}^{N}\left\{\sum_{j=0}^{\left\lfloor\frac{N-l-1}{2}\right\rfloor}\Lambda_{l+2j,j}\,\mathrm{Im}\left[\gamma_{\mathrm{elec}}^{(l+2j)}\gamma_{\mathrm{elec}}^{(l+2j+1)*}\right]+\sum_{j=0}^{\left\lfloor\frac{N-l-2}{2}\right\rfloor}\Omega_{l+2j+1,j}\,\mathrm{Im}\left[\gamma_{\mathrm{elec}}^{(l+2j+1)}\gamma_{\mathrm{elec}}^{(l+2j+2)*}\right]\right\}\mathrm{Im}\,\mathbf{S}_{\mathrm{em}}^{(l)}, \qquad [S4.13]$$

$$\mathbf{F}_{\mathrm{IPM}}^{\mathrm{m}(N)}=-\frac{\mu}{4\pi\varepsilon c^3}\sum_{l=1}^{N}\left\{\sum_{j=0}^{\left\lfloor\frac{N-l-1}{2}\right\rfloor}\Lambda_{l+2j,j}\,\mathrm{Im}\left[\gamma_{\mathrm{mag}}^{(l+2j)}\gamma_{\mathrm{mag}}^{(l+2j+1)*}\right]+\sum_{j=0}^{\left\lfloor\frac{N-l-2}{2}\right\rfloor}\Omega_{l+2j+1,j}\,\mathrm{Im}\left[\gamma_{\mathrm{mag}}^{(l+2j+1)}\gamma_{\mathrm{mag}}^{(l+2j+2)*}\right]\right\}\mathrm{Im}\,\mathbf{S}_{\mathrm{em}}^{(l)}, \qquad [S4.14]$$

$$\begin{aligned}
\mathbf{F}_{\mathrm{IPM}}^{\mathrm{x}(N)}=\frac{\mu}{4\pi\varepsilon c}\sum_{l=1}^{N}\left\{\right.&\sum_{j=0}^{\left\lfloor\frac{N-l}{2}\right\rfloor}M_{l+2j,j}\,\mathrm{Im}\left[\gamma_{\mathrm{elec}}^{(l+2j)*}\gamma_{\mathrm{mag}}^{(l+2j)}\right]-\frac{lk^2}{(l+1)^2}\sum_{j=0}^{\left\lfloor\frac{N-l-1}{2}\right\rfloor}M_{l+2j+1,j}\,\mathrm{Im}\left[\gamma_{\mathrm{elec}}^{(l+2j+1)*}\gamma_{\mathrm{mag}}^{(l+2j+1)}\right]\\
&\left.-\frac{l(l+1)k^4}{(l+2)^2}\sum_{j=0}^{\left\lfloor\frac{N-l-2}{2}\right\rfloor}M_{l+2j+2,j}\,\mathrm{Im}\left[\gamma_{\mathrm{elec}}^{(l+2j+2)*}\gamma_{\mathrm{mag}}^{(l+2j+2)}\right]\right\}\mathrm{Im}\,\mathbf{S}_{\mathrm{em}}^{(l)},
\end{aligned} \qquad [S4.15]$$

Ultimately, it is straightforward to express the IPM force as

$$\mathbf{F}_{\mathrm{IPM}}^{(N)}=\sum_{l=1}^{N}\left(A_{N,l}^{\mathrm{e}}+A_{N,l}^{\mathrm{m}}+A_{N,l}^{\mathrm{x}}\right)\mathrm{Im}\,\mathbf{S}_{\mathrm{em}}^{(l)}. \qquad [S4.16]$$

where $A_{N,l}^{\mathrm{e}}$, $A_{N,l}^{\mathrm{m}}$, $A_{N,l}^{\mathrm{x}}$ are respectively the prefactors in Eqs. [S4.13]-[S4.15] and they are given by Eq. [19] in the main text. In the same manner one may work out the coefficients, $B_{N,l}\sim F_{N,l}$, for the gradient force, radiation pressure and canonical radiation pressure.

Figures S3a-c show the electric, magnetic and hybrid components of the IPM force, calculated with Eqs. [S4.13-4.15] for the particle in Fig. 2c. Note that all the components are in the azimuthal direction (as they should). The electric and magnetic components are always zero for $N = 1$, because the generation of IPM force requires the interaction between different multipoles. At both trapping positions, the electric component $F_{\mathrm{IPM}}^{\mathrm{e(N)}}$ is significant only for $N = 7$, while the magnetic one $F_{\mathrm{IPM}}^{\mathrm{m(N)}}$ is always small, although the latter can reach a remarkable magnitude up to 26.4 pN/W at $\rho = 4.8$ μm, when all multipoles are included. The hybrid component $F_{\mathrm{IPM}}^{\mathrm{x(N)}}$ is nonzero for $N = 1$, and it can be significant for $N > 4$ at the trapping positions. Summing over these lines, we obtain the total IPM force for each N (Fig. S3d). We see that the results are totally consistent with Fig. 2c, verifying our argument that the azimuthal force in Fig. 2c is attributed to the IPM optomechanics. It also validates our Eqs. [S4.13-15] or Eq. [20] in the manuscript.

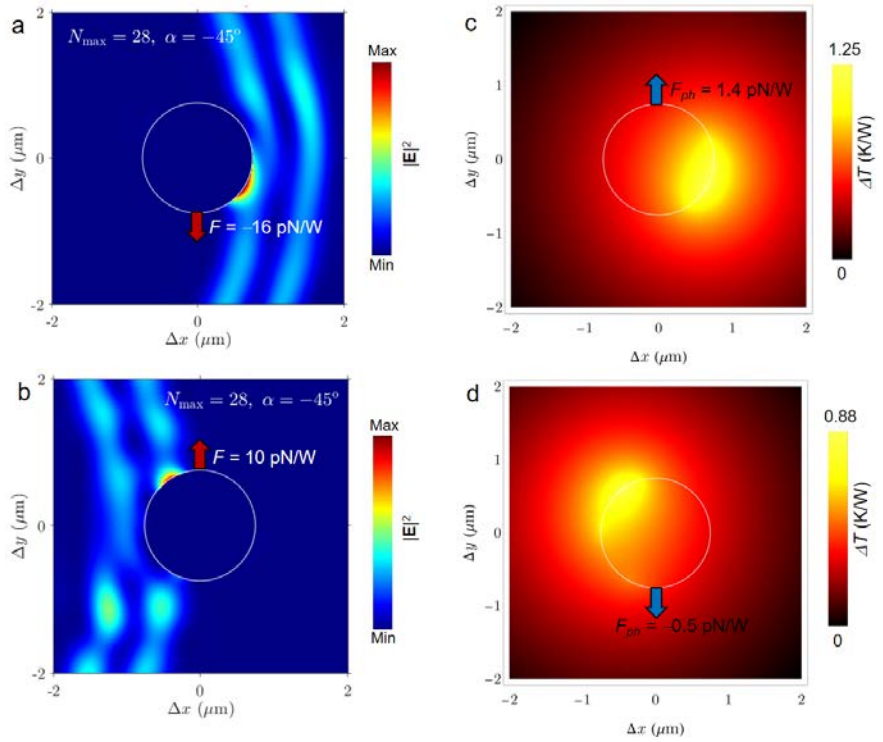

Fig. S1. a,b, Field distribution around the particle for IRT (**a**) and ORT (**b**). Arrows indicate the direction of the optical force *F* acting on the particle. **c,d,** Induced temperature increase ΔT for IRT (**c**) and ORT (**d**). Arrows showing the azimuthal photophoretic force F_{ph}.

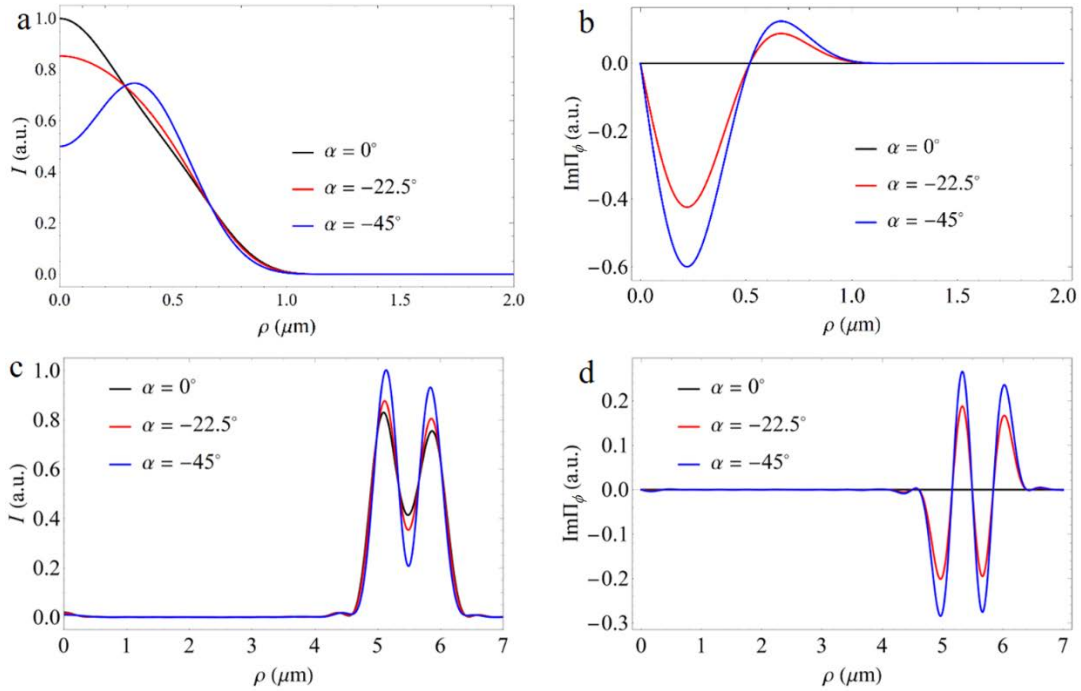

Fig. S2. Comparison of focused field distributions without and with phase modulation. **a,b,** Focused field intensity (**a**) and imaginary Poynting vector (**b**) as a function of the radial position for a standard CV beam input. **c,d,** Similar plots for a CV beam input with a phase modulation factor ρ_0 = 5.5 μm.

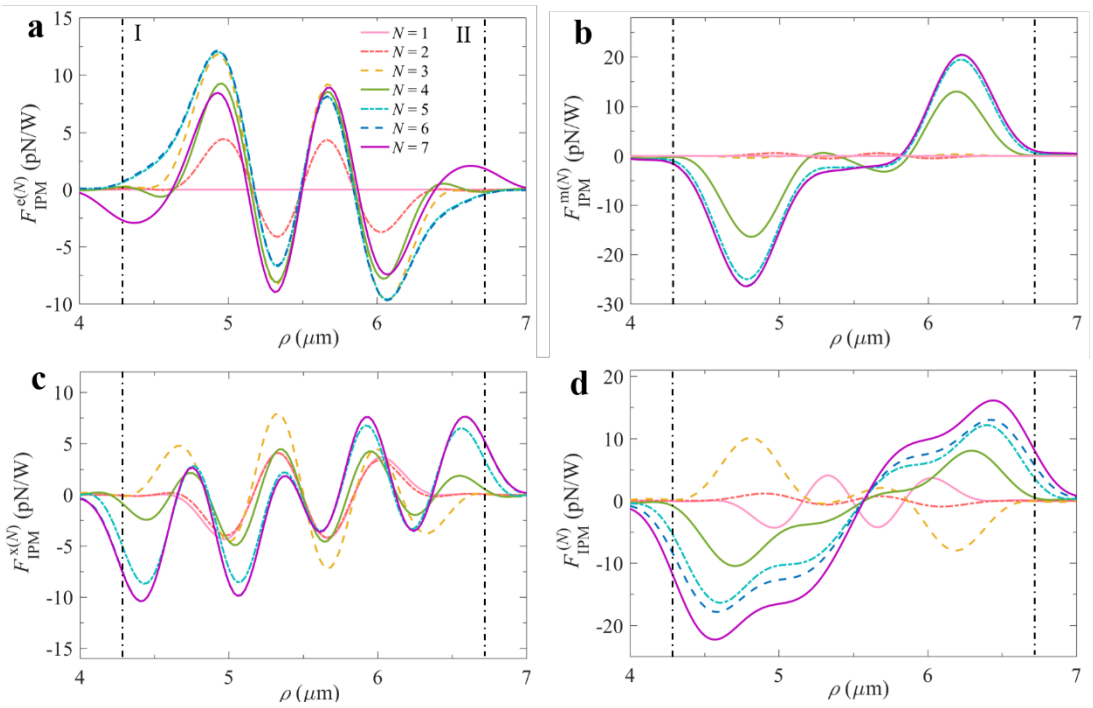

Fig. S3. Calculated electric (**a**), magnetic (**b**) and hybrid (**c**) components of the IPM force versus the radial position of the particle in Fig. 2. The total IPM force (**d**) is obtained by summing over its components in (**a**-**c**) for each *N*, which reproduces the azimuthal force results in Fig. 2c. The vertical dashed line marks the trapping positions I and II determined from Fig. 2a.

Movie S1 (separate file). Simultaneous rotation of two Au particles separately trapped at inner and outer radial equilibrium positions in the focused IPM vortex with polarization parameter α = −45°.

Movie S2 (separate file). Rotation of the Au particle trapped at inner radial equilibrium position in the focused IPM vortex as a function of polarization parameter α.

Movie S3 (separate file). Rotation of the Au particle trapped at outer radial equilibrium position in the focused IPM vortex as a function of polarization parameter α.

SI References

S1. B. Richards, E. Wolf, Electromagnetic diffraction in optical systems II. Structure of the image field in an aplanatic system. *Proc. Roy. Soc. A* 253, 358-379 (1959).

S2. K. S. Youngworth, T. G. Brown, Focusing of high numerical aperture cylindrical vector beams. *Opt. Express* 7, 77–87 (2000).

S3. X. Chen, Y. T. Chen, M. Yan, M. Qiu, Nanosecond photothermal effects in plasmonic nanostructures *ACS Nano* **6**, 2550-2557 (2012).

S4. J. Lu, H. Yang, L. Zhou, Y. Yang, S. Luo, Q. Li, M. Qiu, Light-induced pulling and pushing by the synergic effect of optical force and photophoretic force. *Phys. Rev. Lett.* 118, 043601 (2017).

S5. Q. Zhan, Cylindrical vector beams: from mathematical concepts to applications. *Adv. Opt. Photon.* 1, 1-57 (2009).
S6. M. I. Mishchenko, L. D. Travis, A. A. Lacis, *Scattering, Absorption, and Emission of Light by Small Particles* (Cambridge University Press, Cambridge, 2002).
S7. J. D. Jackson, *Classical Electrodynamics* (Wiley, New York, 1962).
S8. J. P. Barton, D. R. Alexander, S. A. Schaub, Theoretical determination of net radiation force and torque for a spherical particle illuminated by a focused laser beam. *J. Appl. Phys.* 66, 4594–4602 (1989).
S9. Y. Jiang, J. Chen, J. Ng, Z. Lin, Decomposition of optical force into conservative and nonconservative components. arXiv:1604.05138.
S10. H. Zheng, X. Yu, W. Lu, J. Ng, Z. Lin, GCforce: decomposition of optical force into gradient and scattering parts. *Comput. Phys. Commun.* 237, 188-198 (2019).